JACS
JOURNAL OF THE AMERICAN CHEMICAL SOCIETY
Article
pubs.acs.org/JACS

Concurrent Modulation of Quantum Dot Photoluminescence Using a Combination of Charge Transfer and Förster Resonance Energy Transfer: Competitive Quenching and Multiplexed Biosensing Modality

W. Russ Algar,*[,†] Ani Khachatrian,[‡,⊥] Joseph S. Melinger,[‡] Alan L. Huston,[∥] Michael H. Stewart,[∥] Kimihiro Susumu,[∥,⊥] Juan B. Blanco-Canosa,[#] Eunkeu Oh,[∥,⊥] Philip E. Dawson,[#] and Igor L. Medintz[§]

[†]Department of Chemistry, University of British Columbia, Vancouver, BC, V6T 1Z1, Canada

[‡]Electronic Science and Technology Division, Code 6800, [§]Center for Bio/Molecular Science and Engineering, Code 6900, and [∥]Optical Sciences Division, Code 5611, U.S. Naval Research Laboratory, Washington, DC 20375, United States

[⊥]Sotera Defense Solutions, Columbia, Maryland 21046, United States

[#]Departments of Chemistry and Cell Biology, The Scripps Research Institute, La Jolla, California 92037, United States

Supporting Information

ABSTRACT: An emerging trend with semiconductor quantum dots (QDs) is their use as scaffolds to assemble multiple energy transfer pathways. Examples to date have combined various competitive and sequential Förster resonance energy transfer (FRET) pathways between QDs and fluorescent dyes, luminescent lanthanide complexes, and bioluminescent proteins. Here, we show that the photoluminescence (PL) of QD bioconjugates can also be modulated by a combination of FRET and charge transfer (CT), and characterize the concurrent effects of these mechanistically different pathways using PL measurements at both the ensemble and the single particle level. Peptides were distally labeled with either a fluorescent dye that quenched QD PL through FRET or a ruthenium(II) phenanthroline complex that quenched QD PL through electron transfer. The labeled peptides were assembled around a central CdSe/ZnS QD at different ratios, tuning the relative rates of FRET and CT, which were competitive quenching pathways. The concurrent effects of FRET and CT were predictable from a rate analysis that was calibrated to the isolated effects of each of these pathways. Notably, the dye/QD PL intensity ratio reflected changes in the relative rate of FRET but was approximately independent of CT. In turn, the sum of the QD and dye PL intensities, when adjusted for quantum yields, reflected changes in the relative rate of CT quenching, approximately independent of FRET. The capacity for multiplexed sensing of protease activity was demonstrated using these two orthogonal detection channels. Combined CT-FRET configurations with QDs are thus promising for applications in bioanalysis, sensing, and imaging, and may prove useful in other photonic applications.

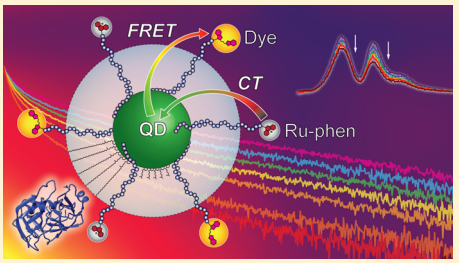

INTRODUCTION

Colloidal semiconductor nanocrystals, or "quantum dots" (QDs), remain a benchmark against which many other photoluminescent materials are measured. In the context of bioanalysis and bioimaging, their favorable optical properties include spectrally broad light absorption, spectrally narrow photoluminescence (PL) that can be tuned through nanocrystal size and composition, large one- and two-photon absorption cross sections, good quantum yields, and resistance to photobleaching.[1−3] Further value is derived from their small size (typically <10 nm) and the wide variety of established methods for surface functionalization and bioconjugation.[4,5] These features are so advantageous that a multitude of biological applications of QDs have been reported in the literature,[6−8] along with sustained efforts to synthesize QDs from more benign materials than the classic CdX (X = S, Se, Te) semiconductors.[9−12] The continued development of biofunctional QDs is expected to lead to new probes and technologies for the elucidation of biochemical pathways, the detection of biomarkers, and other biophotonic applications.

An emerging paradigm with QDs is the integration of multiple energy transfer pathways around a central QD scaffold,[13] and several biophotonic embodiments of this concept have been reported. Some of the first examples were multivalent assemblies of photonic wires, where the QD served as a light harvesting antenna and scaffold for double-stranded DNA that was labeled with a series of fluorophores.[14,15] The QD, acting as a FRET donor, initiated an energy transfer cascade down the length of the labeled DNA. Another development has been the use of QDs in two roles—as both acceptor and donor—in energy transfer relays.[16−19] QDs are initially sensitized as acceptors for a luminescent lanthanide donor and subsequently serve as a donor for a fluorescent dye

Received: October 22, 2016
Published: December 23, 2016

DOI: 10.1021/jacs.6b11042
J. Am. Chem. Soc. 2017, 139, 363−372

acceptor, where both the lanthanide complex and the dye are assembled to a common QD. This format has been the basis of probe configurations for sensing and biophotonic logic.[16−19] A variation on this concept has utilized an initial bioluminescence resonance energy transfer (BRET) step to a QD acceptor, which then serves as a donor for a fluorescent protein[20] or a DNA photonic wire.[21] Another important development has been "concentric" FRET configurations, which assemble a central QD donor with two different fluorescent dye acceptors.[22] These configurations have multiple FRET pathways that are both competitive and sequential, and are promising for multiplexed biological sensing and imaging.[23−25] Photochromic configurations with multiple energy transfer pathways have also been developed, with both a conventional fluorescent dye and a photochromic dye coassembled around a central QD.[26]

A common element between the foregoing configurations is putative dipolar energy transfer through a FRET mechanism. Seminal work on FRET between QDs and fluorescent dyes,[27,28] fluorescent proteins,[29−31] lanthanide complexes,[32,33] and bioluminescent enzymes[34,35] inspired many subsequent studies, leading to a relatively comprehensive understanding of FRET with QD materials.[13] This understanding has facilitated development of the advanced configurations noted above, as well as a multitude of applications of QDs and FRET, particularly in biological contexts.[13] Another mechanism of PL quenching in QD bioconjugates is charge transfer (CT), albeit less studied, less understood, and less utilized than FRET with QDs.[36] It has been shown that redox active complexes and small molecules such as ruthenium(II) phenanthroline,[37−41] ferrocene,[42] and quinones,[43−45] among other species,[46] can quench the PL of QD bioconjugates through CT, and do so in a manner that is useful for bioanalysis and sensing.[36] Whereas FRET configurations can be rationally designed with the help of measurable optical properties such as absorption and emission spectra, molar absorption coefficients, excited state lifetimes, and quantum yields, the CT quenching process depends on more nuanced factors such as the alignment of energy levels and properties of the QD surface.[36,47] Nonetheless, there is value in the design of optical probes based on the CT quenching of QDs. Prospective and demonstrated advantages include a stronger distance dependence than FRET, "universal" quenching that is free from the requirement of spectral overlap, and sensitivity to biological redox processes.[36,37,48]

Here, we evaluate the combination of CT and FRET within a QD bioconjugate. As illustrated in Figure 1, a CdSe/ZnS core/shell QD with a hydrophilic ligand coating is assembled with multiple copies of two different peptides: a peptide with a distal ruthenium(II) phenanthroline (Ru-phen) label and a peptide with a distal fluorescent dye label. Peptides with distal Ru-phen labels have been established to quench QD PL via electron transfer from the ruthenium(II) center to the QD,[38,39] and dye-labeled peptides are well-known to quench QD PL via FRET.[13] These two pathways are mechanistically different, in contrast to previous studies that have only combined pathways with a common underlying mechanism of dipolar resonance energy transfer. We now show that CT and FRET can coexist as competitive mechanisms of quenching QD PL, the net effect of which can be understood and predicted through a rate analysis. The rates of CT and FRET can be tuned through control of the number of Ru-phen and fluorescent dye moieties per QD, and the dye/QD PL intensity ratio can serve as a signature of FRET, approximately independent of CT. When corrected for quantum yields, the combined PL intensities of the QD and the dye can also serve as a signature of CT quenching, approximately independent of FRET. This configuration is a valuable model system for understanding the combination of CT and FRET, and holds promise for future applications in multiplexed biological sensing and other photonic applications.

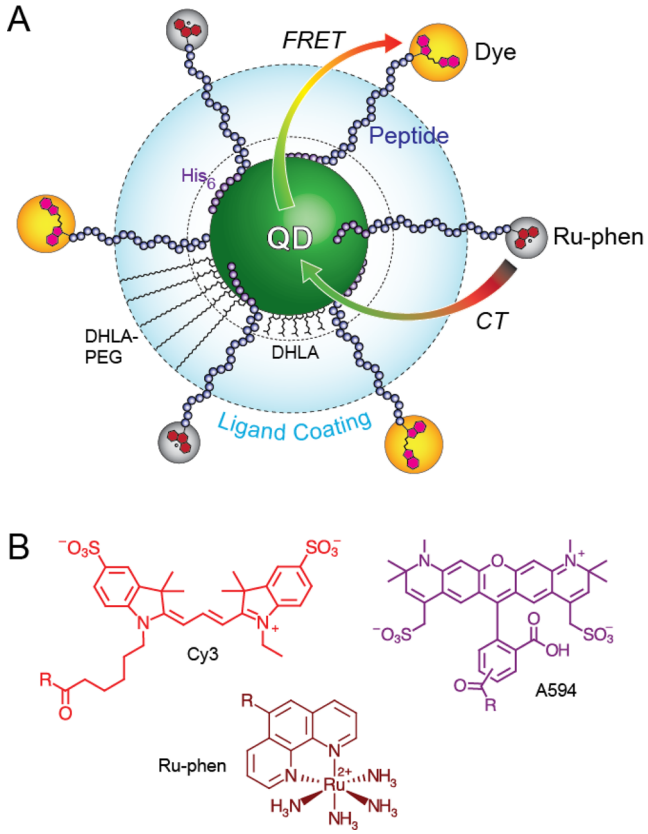

Figure 1. (A) Schematic illustration of the combined CT and FRET system constructed around a central QD using self-assembled polyhistidine-terminated peptides. The peptides are labeled at their distal termini with either a ruthenium(II) phenanthroline complex (Ru-phen) or a fluorescent dye (A555, Cy3, A594). The QD is coated with either DHLA-PEG or DHLA ligands. (B) Molecular structures of Cy3, A594, and Ru-phen. The structure of A555 has not been made available but is thought to be a more sulfonated derivative of Cy3.

RESULTS

QD Conjugates. A QD conjugate with tunable rates of CT and FRET was constructed with polyhistidine-terminated peptides that were labeled with Ru-phen and a fluorescent dye such as cyanine 3 (Cy3), Alexa Fluor 555 (A555), or Alexa Fluor 594 (A594). Molecular structures of the Ru-phen and dyes are shown in Figure 1B. Ru-phen has been shown to quench QD PL as an electron donor,[38,39] and all three dyes were good FRET acceptors for a CdSe/ZnS QD with peak PL emission at ∼520 nm.[22,49] Figure 2 shows the absorption and emission spectra for the QD, Ru-phen, Cy3, A555 (an analogue of Cy3), and A594. Where possible, the system was interrogated with an excitation wavelength that minimized direct excitation of the dyes. Note that the molar absorption coefficient of the QD was either ∼30−40-fold larger (excitation wavelengths 2 and 4 in Figure 2) or more than 350-fold larger (excitation wavelengths 1 and 3 in Figure 2) than the Ru-phen, such that direct photoexcitation of the Ru-phen was unlikely to

DOI: 10.1021/jacs.6b11042
J. Am. Chem. Soc. 2017, 139, 363−372

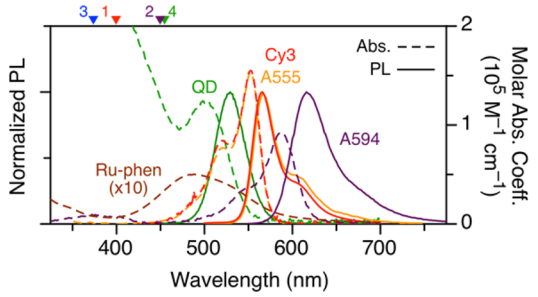

Figure 2. Normalized PL spectra and wavelength-dependent molar absorption coefficients for the QD, Cy3, A555, A594, and Ru-phen. The absorption coefficients for Ru-phen are multiplied by a factor of 10. The Ru-phen did not have measurable emission. The arrows on the top axis indicate the excitation wavelengths for different experiments: (1) PL emission spectra with A555 and Cy3; (2) PL emission with A594; (3) PL lifetime measurements with Cy3; and (4) single-particle FRET measurements with Cy3.

be significant in measurements. The estimated Förster distances for the QD donor paired with Cy3, A555, and A594 acceptors were 5.2, 5.1, and 4.2 nm, respectively (see the Supporting Information for spectral overlap integrals). A555 is thought be a sulfonated cyanine dye derivative, whereas A594 is a xanthene dye derivative. The combination of CT and FRET was thus evaluated with two different classes of fluorescent dye. Control over FRET and CT rates in the system was achieved by varying the number of Ru-phen- and dye-labeled peptides per QD. The peptides were designed with polyhistidine tags, which have been shown to permit efficient self-assembly to ligand-coated QDs with nanomolar dissociation constants, such that the number of peptides per QD was tunable based on mixing stoichiometry.[50,51] We denote QD-peptide conjugates as $[Pep(Ru\text{-}phen)]_M$-QD-$[Pep(dye)]_N$, or (M, N) in shorthand, where M and N are the ensemble average numbers of Ru-phen-labeled peptides and dye-labeled peptides per QD, respectively. These values are averages because peptides assemble to individual QDs according to a Poisson distribution.[52] The sum, $M + N$, was also less than the maximum peptide loading of the QDs.[53] The expected rates of CT and FRET were thus adjustable through control of the values of M and N. Experiments were done with QDs coated with both DHLA-PEG ligands (QD_P) and DHLA ligands (QD_D), for which a prior study has suggested small differences in the details of the charge transfer mechanism.[38]

Combined Quenching of QD PL Intensity. Figure 3A shows representative spectra for $[Pep(Ru\text{-}phen)]_M$-QD_P-$[Pep(Cy3)]_N$ conjugates. As expected, the effect of increasing M was progressive quenching of QD PL, and the effect of increasing N was progressive quenching of QD PL with concomitant FRET sensitization of Cy3 PL. Figure 3A also shows representative spectra for (M, N) combinations where $N \neq 0$ and is constant while M is varied. The effect of increasing N was to decrease the overall intensity of the PL emission spectrum (both QD and dye contributions) with only small changes in the shape of the spectrum (*vide infra*). Figure 3B maps the changes in QD and Cy3 PL as a function of (M, N). Analogous data for $[Pep(Ru\text{-}phen)]_M$-QD_P-$[Pep(A594 \text{ or } A555)]_N$ conjugates can be found in the Supporting Information and showed analogous trends.

The assembly of both Pep(Ru-phen) and Pep(dye) quenched QD PL, with greater quenching observed for a combination of Pep(Ru-phen) and Pep(dye) than for either alone. The QD quenching efficiency, Q_{QD}, thus represented combined contributions from both CT and FRET. The quenching efficiency was calculated from eq 1, where $I_{QD}(M, N)$ is the measured QD PL intensity for a $[Pep(Ru\text{-}phen)]_M$-QD_P-$[Pep(dye)]_N$ conjugate.

$$Q_{QD,meas.} = 1 - \frac{I_{QD}(M, N)}{I_{QD}(0, 0)} \quad (1)$$

Following previous studies on QDs with competitive FRET pathways,[24,26,54] the QD quenching efficiency for nonzero (M, N) combinations was predicted from the expected relative rates of FRET, Γ_{FRET}, and CT, Γ_{CT}. Using eq 2, these rates were derived from fitting of the QD quenching efficiencies for $(0, N)$ and $(M, 0)$ samples, respectively (see the Supporting Information for details). That is, combined quenching by FRET and CT was predicted from measurements of FRET and CT in isolation. Equation 2 is derived from first-principles, where $\Gamma_X = k_{QD}{}^{-1} r_X$, k_{QD} is the intrinsic relaxation rate of the

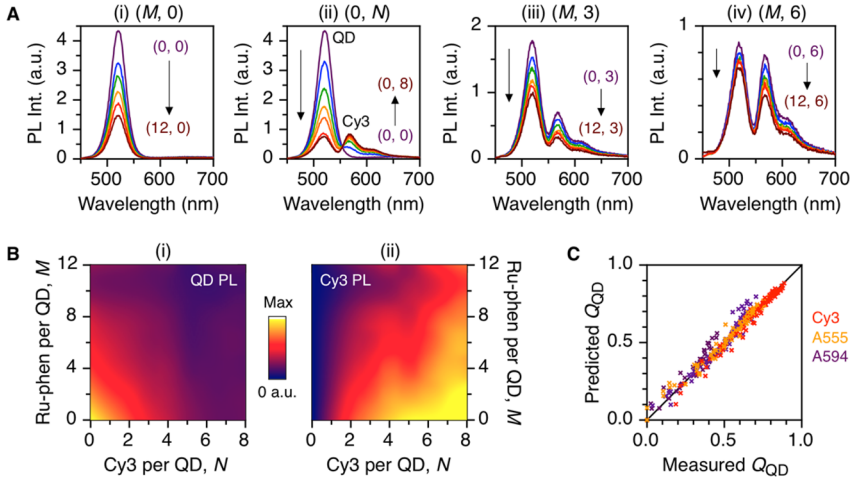

Figure 3. PL intensity measurements of combined CT and FRET quenching of QDs. (A) Representative spectra for select subsets of $[Pep(Ru\text{-}phen)]_M$-QD_P-$[Pep(Cy3)]_N$ conjugates, denoted as (M, N): (i) $(M, 0)$; (ii) $(0, N)$; (iii) $(M, 3)$, and (iv) $(M, 6)$. (B) Representative maps of QD PL intensity (au) and FRET-sensitized Cy3 PL intensity (au) as a function of M and N. (C) Plot of the predicted QD quenching efficiency versus the measured QD quenching for $[Pep(Ru\text{-}phen)]_M$-QD_P-$[Pep(dye)]_N$ conjugates, where the dye is Cy3, A555, or A594. The solid line has unit slope.

DOI: 10.1021/jacs.6b11042
J. Am. Chem. Soc. 2017, 139, 363−372

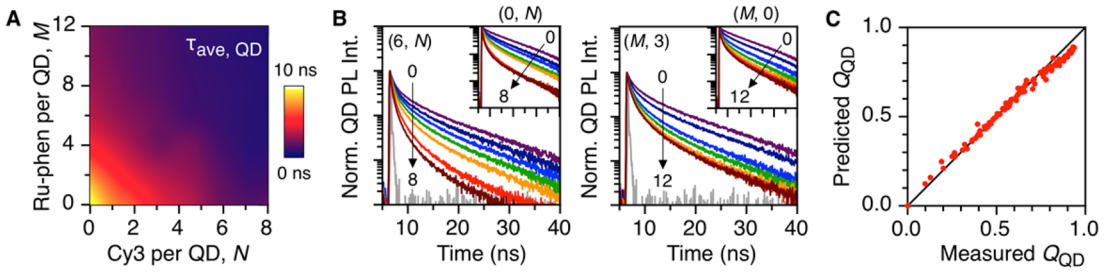

Figure 4. PL lifetime measurements of combined CT and FRET quenching of QDs. (A) Representative QD PL lifetime map for $[Pep(Ru\text{-}phen)]_M$-QD_P-$[Pep(Cy3)]_N$ conjugates as a function of M and N. (B) Representative QD PL decay curves for select subsets of $[Pep(Ru\text{-}phen)]_M$-QD_P-$[Pep(Cy3)]_N$ conjugates, denoted as (M, N): (6, N), (0, N), (M, 3), and (M, 0). The instrument response function is shown in gray in the main panels. (C) Plot of the predicted QD quenching efficiency versus the measured QD quenching for $[Pep(Ru\text{-}phen)]_M$-QD_P-$[Pep(Cy3)]_N$ conjugates. The solid line has unit slope.

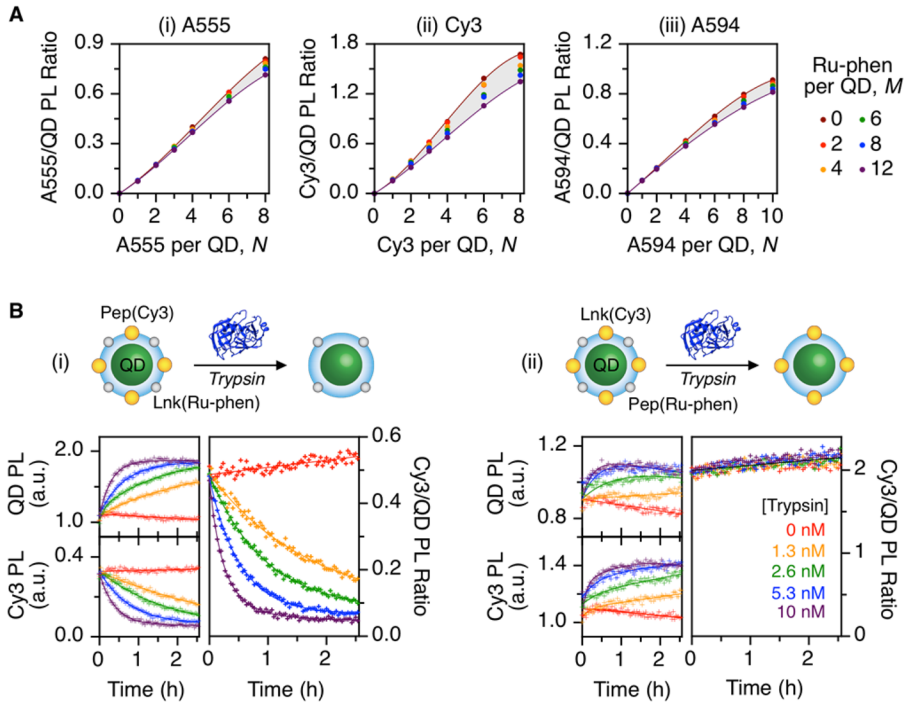

Figure 5. Dye/QD PL ratio as a function of the number of Ru per QD. (A) Dye/QD PL ratios for $[Pep(Ru\text{-}phen)]_M$-QD_P-$[Pep(dye)]_N$ conjugates with (i) A555, (ii) Cy3, and (iii) A594 dyes, as a function of M and N. The shaded region represents the spread of the data. The observed PL ratio decreased slightly as M increased, especially at larger values of N. (B) Enzymatic hydrolysis of (i) $[Lnk(Ru\text{-}phen)]_3$-QD_P-$[Pep(Cy3)]_5$ and (ii) $[Pep(Ru\text{-}phen)]_7$-QD_P-$[Lnk(Cy3)]_3$ conjugates using increasing concentrations of trypsin, which hydrolyzed either Pep(Cy3) or Pep(Ru-phen) in the experiments, but not Lnk(Ru-phen) or Lnk(Cy3). In (i), the Cy3 was cleaved from the QD with gradual loss of FRET. In (ii), the Ru-phen was cleaved from the QD with gradual loss of CT. The time-dependent changes in QD PL, Cy3 PL, and Cy3/QD PL ratio are shown for both experiments. The PL ratio changed with loss of FRET but did not change with loss of CT.

QD (sum of radiative and nonradiative rates), and r_X is the rate of X = CT or FRET.

$$Q_{QD,pred.} = \frac{\Gamma_{CT} + \Gamma_{FRET}}{1 + \Gamma_{CT} + \Gamma_{FRET}} \quad (2)$$

As shown in Figure 3C, data points on plots of the predicted QD quenching efficiency (eq 2) versus the experimentally measured quenching efficiency largely fell on a line with unit slope for the combination of Ru-phen and Cy3. Results are also plotted for analogous experiments with A555 and A594 combined with Ru-phen (see the Supporting Information, Figures S3 and S4, for PL data), and these trends also fell on the line with unit slope. These results indicated that eq 2, a model based on competing rates of CT and FRET, accurately predicted the observed ensemble quenching of the QD. Although the results in Figure 3 are for DHLA-PEG-coated QDs, additional experiments with DHLA-coated QDs showed analogous trends, albeit shifted to higher values of Q_{QD} (see the Supporting Information, Figures S5 and S6).

Combined Quenching of QD PL Lifetime. As FRET and CT compete with the intrinsic radiative and nonradiative relaxation mechanisms of the QD, a decrease in QD PL lifetime was expected with increasing M and N. Indeed, the experimental QD PL decay rate increased as both M and N increased, and the amplitude-weighted lifetimes (from modeling the decays as biexponential) are mapped as a function of (M, N) in Figure 4A. Representative PL decay curves for different (M, N) combinations with $[Pep(Ru\text{-}phen)]_M$-QD_P-$[Pep(Cy3)]_N$ conjugates are shown in Figure 4B. The QD PL

DOI: 10.1021/jacs.6b11042
J. Am. Chem. Soc. 2017, 139, 363−372

quenching efficiency was measured from changes in the average QD PL lifetime, $\tau_{ave,QD}$, as per eq 3:

$$Q_{QD,meas.} = 1 - \frac{\tau_{ave,QD}(M, N)}{\tau_{ave,QD}(0, 0)} \quad (3)$$

As before, the QD PL quenching was predicted from eq 2, with calibration of Γ_{FRET} and Γ_{CT} from fitting of the lifetime-derived QD quenching efficiencies for (0, N) and (M, 0) samples. Figure 4C plots the predicted QD quenching efficiency versus the measured quenching efficiency, with all data derived from QD PL lifetimes. As with the analogous intensity data (see Figure 3C), the lifetime data fell on a line with unit slope, indicating good agreement between predictions and measurements. Lifetime data obtained with DHLA-coated QDs followed the same trends, once again shifted to higher values of Q_{QD} (see the Supporting Information, Figure S7). From the DHLA-PEG-coated QD lifetime for the (0, 0) sample, for which k_{QD} = 0.094 ns^{-1}, and accommodating batch-to-batch variations in experiments, the average absolute rate of CT per Ru-phen was typically in the range 0.004−0.02 ns^{-1}, whereas the average absolute rates of FRET per dye were typically 0.005−0.01 ns^{-1} for A594 and 0.02−0.05 ns^{-1} for A555 and Cy3. For DHLA-coated QDs, k_{QD} = 0.10 ns^{-1}, the average absolute rate of CT per Ru-phen was typically between 0.02 and 0.2 ns^{-1}, and the average absolute rates of FRET per dye were between 0.09 and 0.15 ns^{-1} for A594 and between 0.06 and 0.3 ns^{-1} for A555 and Cy3.

PL Ratios. A characteristic and analytically useful attribute of FRET with fluorescent dye acceptors is FRET-sensitized emission from that acceptor. With the effect of CT on the QD PL emission characterized, it was important to evaluate the effect of CT on the acceptor dye PL. The ratio of acceptor dye and QD PL emission, I_{dye}/I_{QD}, was expected to follow eq 4, which is derived in the Supporting Information. The main result of eq 4 is that the PL ratio was expected to be independent of CT, and thus independent of M, the average number of Ru-phen per QD.

$$\frac{I_{dye}}{I_{QD}} = \left(\frac{\Phi_{dye}}{\Phi_{QD}}\right)\left(\frac{E_{FRET}}{1 - Q_{QD}}\right) = \left(\frac{\Phi_{dye}}{\Phi_{QD}}\right)\Gamma_{FRET} \quad (4)$$

Figure 5A shows representative examples of plots of dye/QD PL ratios for $[Pep(Ru\text{-}phen)]_M$-QD_P-$[Pep(dye)]_N$ conjugates as a function of M and N, where the dye was A555, Cy3, or A594. The plots show that the PL ratio was largely independent of M at lower values of M and N, with deviations from uniformity increasing as both M and N became larger. In the case of A555 and A594, the maximum deviation was less than 15%, whereas for the Cy3 the deviation reached a maximum of 25%.

In light of the small variations in PL ratio with preparation of different (M, N) samples, an experiment was devised to change the number of Ru-phen per QD without changing the number of peptides and without preparing different samples. Rather than assembling Ru-phen and Cy3 to the QD through equivalent peptide linkers, the Ru-phen and Cy3 were assembled through two different peptide linkers. The peptide linker for the Ru-phen (or Cy3) remained unchanged as a 29-residue sequence with arginine and lysine residues that trypsin, a proteolytic enzyme, was able to site-selectively recognize and hydrolyze. In contrast, the peptide linker for Cy3 (or Ru-phen) was changed to a much shorter, 15-residue peptide that was very resistant to hydrolysis by trypsin because it did not contain lysine or arginine residues. This peptide linker is denoted as Lnk(Cy3) (or Lnk(Ru-phen)). Figure 5B illustrates these experiments and shows representative results with different concentrations of trypsin added to either $[Pep(Ru\text{-}phen)]_M$-QD_P-$[Lnk(Cy3)]_N$ or $[Lnk(Ru\text{-}phen)]_M$-QD_P-$[Pep(Cy3)]_N$ conjugates. As the concentration of trypsin increased, the measured Cy3/QD PL ratio for $[Pep(Ru\text{-}phen)]_M$-QD_P-$[Lnk(Cy3)]_N$ conjugates remained constant, although the individual QD and Cy3 PL signals increased. With trypsin and $[Lnk(Ru\text{-}phen)]_M$-QD_P-$[Pep(Cy3)]_N$ conjugates, the QD PL signal increased with a parallel decrease in the Cy3 PL signal, and thus a decrease in the Cy3/QD PL ratio. Equivalent trends were observed with DHLA-coated QDs (see the Supporting Information, Figure S8). Overall, these results confirmed that the dye/QD PL ratio was approximately independent of the CT rate, and that the small changes in PL ratio in Figure 5A were likely due to other factors (see the Discussion section).

Single-Particle FRET Measurements. To further study the effect of CT on the QD and dye PL, single particle FRET measurements were made on $[Pep(Ru\text{-}phen)]_M$-$QD_{P/D}$-$[Pep(Cy3)]_N$ conjugates in bulk solution. Bursts of QD and Cy3 PL were recorded as individual conjugates diffused through a confocal detection volume. Summary histograms of the $I_{Cy3}/(I_{QD} + I_{Cy3})$ ratios are shown in Figure 6A for DHLA-coated QDs, where I_{Cy3} and I_{QD} are the PL burst intensities in the Cy3 and QD detection channels, respectively. Analogous data for DHLA-PEG-coated QDs is shown in the Supporting Information (see Figure S9). In both cases, the histograms varied significantly in shape with changes in N, the number of Cy3 per QD, but had much smaller variations in shape with

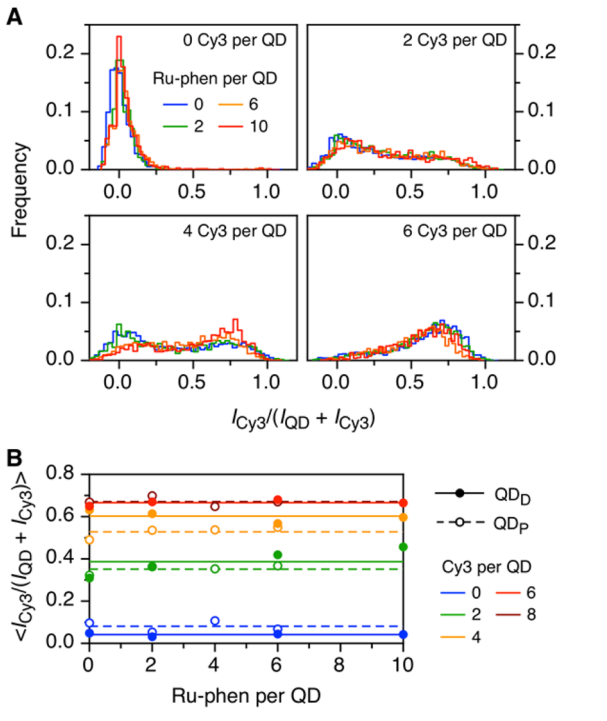

Figure 6. Single particle measurements of CT and FRET. (A) Histograms for the $I_{Cy3}/(I_{QD} + I_{Cy3})$ PL ratio for different values of M and N with $[Pep(Ru\text{-}phen)]_M$-QD_D-$[Pep(Cy3)]_N$ conjugates in bulk solution. (B) Summary of the average $I_{Cy3}/(I_{QD} + I_{Cy3})$ PL ratios for both DHLA-coated QDs (QD_D) and DHLA-PEG-coated QDs (QD_P).

DOI: 10.1021/jacs.6b11042
J. Am. Chem. Soc. 2017, 139, 363−372

changes in M, the number of Ru-phen per QD (for a fixed value of N). Figure 6B plots the average $I_{Cy3}/(I_{QD} + I_{Cy3})$ ratio measured as a function of M and N for both the DHLA-coated QDs and the DHLA-PEG-coated QDs. The values were approximately constant as a function of M, in good agreement with the ensemble results for the Cy3/QD PL ratios.

DISCUSSION

Competitive Dynamic Quenching. PL quenching can be subdivided into static and dynamic mechanisms, where the latter act on the excited state of an emitter and decrease its PL lifetime.[55] Here, dynamic quenching should not be misinterpreted as quenching through diffusion-mediated collisions. The QD, dyes, and Ru-phen are bound to one another in our system. As Figure 4 shows, the QD PL lifetime progressively decreased with increased CT quenching by Ru-phen (consistent with previous results[38,39]) and with increased FRET to a fluorescent dye acceptor. CT between the QD and the dyes can almost certainly be ruled out because of the large spectral overlaps and the large expected average distance between the QD and peptide-linked dyes.[56] Figure 7 is a qualitative energy level diagram of a photoexcited QD with proximal Ru-phen and fluorescent dye molecules. After excitation, the isolated QD relaxes to its ground state via its intrinsic nonradiative and radiative mechanisms, with a net rate denoted by k_{QD}. Assembly of Ru-phen to the QD introduces a second relaxation pathway, which is putative electron transfer from the HOMO of the Ru-phen to the photogenerated hole in the quantum confined valence band edge state of the QD. This initial electron transfer, which converts Ru-phen from the +2 oxidation state to the +3 oxidation state, is putatively followed by electron transfer from the quantum confined conduction band edge state of the QD to regenerate the +2 oxidation state (not shown in Figure 7).[36,39] The rate of CT quenching per Ru-phen is k_{CT}, which integrates to r_{CT} over all M Ru-phen moieties per QD. Likewise, the assembly of a dye acceptor introduces energy transfer through dipolar coupling and FRET as a third mechanism of relaxation. The rate of FRET per dye is k_{FRET}, which integrates to r_{FRET} over all M moieties per QD. Equation 2 was derived from the premise that the intrinsic, CT, and FRET mechanisms of relaxation competed with one another, and the validity of this equation was borne out by the results of experiments where M and N were varied. Although a previous study found evidence of a different balance of roles in CT for the core states and surface states of QDs when coated with DHLA versus DHLA-PEG ligands,[38] we did not observe any significant difference between QD_D and QD_P conjugates in combined CT-FRET configurations. The consistently lower FRET and CT efficiencies with QD_P versus QD_D was presumably a result of larger average QD-dye/Ru-phen separations imposed by the steric bulk of the DHLA-PEG ligands versus the compact DHLA ligands.

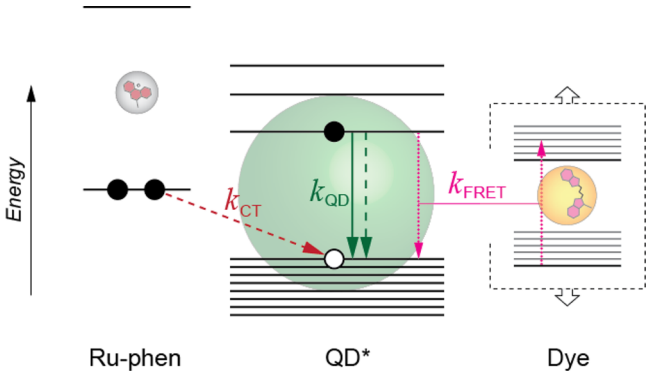

Figure 7. Qualitative energy level diagram for combined CT and FRET quenching of QD PL. The rate of electron transfer from the HOMO of Ru-phen to the photogenerated hole in the quantum confined valence band edge state of the QD, k_{CT}, competes with the rate of FRET, k_{FRET}, and the intrinsic relaxation rate of the QD, k_{QD}. Radiative pathways are shown as solid lines. Nonradiative pathways are shown as dashed lines. The dipolar coupling and transitions associated with FRET are shown as dotted lines. Electrons and holes are illustrated as filled and open circles, respectively. The initial electron transfer from the Ru-phen to the QD is presumed to be followed by a transfer from the quantum confined conduction band edge state of the QD to Ru-phen to restore the ground state of both species (not shown). The figure is not intended to illustrate the alignment of the energy levels of the three different dyes utilized. Any possible role of surface states in the CT process is also not shown.

The use of $(M, 0)$ and $(0, N)$ data to calibrate r_{CT} and r_{FRET} mirrored a rate analysis framework that we have previously used to analyze concentric FRET configurations.[24,54] In an ideal FRET or CT system with multiple and equivalent dye or Ru-phen moieties per QD, the net rate of quenching would follow $r_X = Yk_X$, where X = CT or FRET and $Y = M$ or N. As detailed in the Supporting Information, the quenching rates did not scale linearly in the $(M, 0)$ and $(0, N)$ configurations, indicating that each assembled dye or Ru-phen per QD was not strictly equivalent. The trends with M or N had a slight upward curvature at lower values and/or tended toward a plateau at higher values, and were thus fit with empirical polynomial functions. Such nonlinear trends have been observed in QD-FRET systems previously[54] and reflect the complexity of real versus ideal systems. Possible contributions to nonideal behavior include peptide-loading-dependent changes in QD quantum yield (from greater surface passivation[28]) or the conformation of assembled peptides (increase in QD-dye and QD-Ru-phen distances), the Poisson statistics of assembly at low numbers of peptide per QD (especially for M, $N < 4$),[52] and inequivalent binding sites for peptides on the nanocrystal surface, among other possibilities. Successful prediction of combined CT and FRET quenching efficiencies using eq 2 is evidence of the robustness of the calibrated rate analysis.

Toward Multiplexed Protease Sensing. An outcome of the rate analysis in eq 2 is that the ratio of FRET-sensitized dye PL and QD PL should be independent of CT. Ensemble and single particle FRET experiments largely confirmed this result in the real system, with the exception of small variations in the dye/QD PL ratio at higher values of M and N in Figure 5A. Given the results of experiments with enzymatic hydrolysis of Ru-phen- and dye-labeled peptides in Figure 5B, the variations in Figure 5A appear to have been primarily due to inequivalences introduced in a real system by changing the number of peptides per QD (*vide supra*). Another possibility that we considered was that Ru-phen could quench the PL of coassembled dyes, but significant and consistent quenching effects were not observed when the dyes were directly photoexcited (see the Supporting Information, Figure S10). Aside from the quantitative derivation from the rate analysis, the constant dye/QD PL ratio can be understood as a consequence of the fact that CT competed with both FRET and the intrinsic relaxation pathways of the QD, such that the relative numbers of intrinsic relaxation events and FRET events decreased in parallel.

DOI: 10.1021/jacs.6b11042
J. Am. Chem. Soc. 2017, 139, 363−372

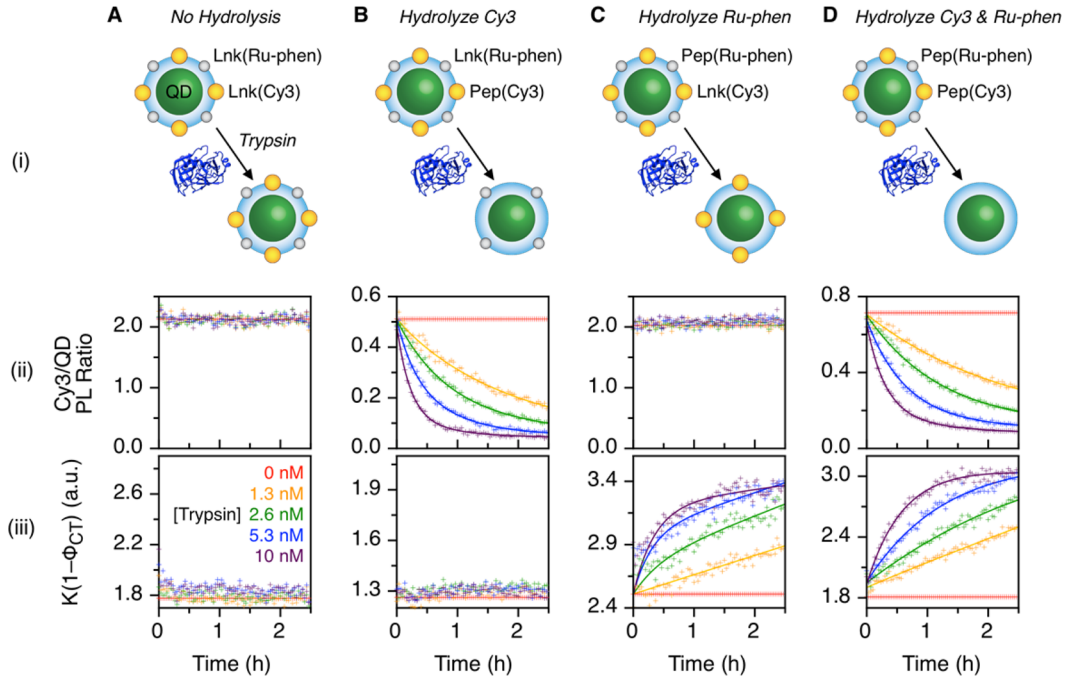

Figure 8. Orthogonal detection of the proteolytic activity of trypsin in different configurations combining CT and FRET: (A) $[Lnk(Ru\text{-}phen)]_3$-QD_P-$[Lnk(Cy3)]_3$, (B) $[Lnk(Ru\text{-}phen)]_3$-QD_P-$[Pep(Cy3)]_5$, (C) $[Pep(Ru\text{-}phen)]_7$-QD_P-$[Lnk(Cy3)]_3$, and (D) $[Pep(Ru\text{-}phen)]_7$-QD_P-$[Pep(Cy3)]_5$. The figure shows (i) a schematic of the experiment, (ii) progress curves in terms of the Cy3/QD PL ratio, and (iii) progress curves in terms of the $K(1 - \Phi_{CT})$ value. The progress curves were normalized to the control samples with no trypsin (0 nM). K is the proportionality between the measured PL intensity (in arbitrary units) and $(1 - \Phi_{CT})$.

Given that the dye/QD PL ratio had a strong dependence on FRET and little or no dependence on CT, the dye/QD PL ratio can be used as an analytical signal to track events or processes that affect FRET. If a metric that were sensitive to changes in CT but insensitive to changes in FRET could be found, then the combination of CT and FRET would permit orthogonal sensing of two processes, analogous to what has been achieved with concentric FRET configurations.[22−25] A possible metric for this purpose is the number of excitation events that do not lead to CT. One fraction of these excitation events dissipates energy at the QD through both radiative and nonradiative mechanisms; the other fraction of excitation events is transferred to the dye via FRET, where energy is also dissipated at the dye through radiative and nonradiative mechanisms. The PL intensity measured from the QD and dye is proportional to the fraction of these excitation events that are dissipated radiatively, and the total number of events can be determined by using quantum yields to account for events that are dissipated nonradiatively. The number of excitation events that do not lead to CT, $(1 - \Phi_{CT})$, can be estimated from eq 5, where Φ_{CT} is the quantum yield of CT, defined by eq 6, and Φ_{dye} and Φ_{QD} are the intrinsic quantum yields of the dye and QD (that is, the quantum yield of the QD donor in the absence of FRET and CT).

$$(1 - \Phi_{CT}) \propto \frac{I_{QD}}{\Phi_{QD}} + \frac{I_{dye}}{\Phi_{dye}} \tag{5}$$

$$\Phi_{CT} = \frac{\Gamma_{CT}}{1 + \Gamma_{FRET} + \Gamma_{CT}} \tag{6}$$

With eq 5, the data in Figure 5B can be reanalyzed, along with additional data that was collected in parallel. In addition to the configurations in Figure 5B, where either Ru-phen or Cy3 was enzymatically cleaved from the QD, measurements were also made with configurations where neither or both of Ru-phen and Cy3 were cleaved. Figure 8 illustrates these configurations and changes in their Cy3/QD PL ratios and $K(1 - \Phi_{CT})$ values, where K is an arbitrary constant that makes eq 5 an equality. In the configuration where only Cy3 was cleaved, the Cy3/QD PL ratio decreased and $K(1 - \Phi_{CT})$ was approximately constant. In contrast, in the configuration where only Ru-phen was cleaved, the Cy3/QD PL ratio was constant and $K(1 - \Phi_{CT})$ increased. The Cy3/QD PL ratio and $K(1 - \Phi_{CT})$ decreased and increased in parallel in the configuration where both Cy3 and Ru-phen were cleaved. The data and Figure 8 thus show that the Cy3/QD PL ratio and $K(1 - \Phi_{CT})$ are two orthogonal signals with the potential to enable multiplexed sensing of, for example, the activity of two different proteases. Although the data in Figure 8 is for DHLA-PEG-coated QDs, analogous data was obtained with DHLA-coated QDs (see the Supporting Information, Figure S11). With the DHLA-PEG configurations, it was found that values of $\Phi_{QD} = 0.15$ and $\Phi_{Cy3} = 0.09$ yielded orthogonal signals, whereas values of $\Phi_{QD} = 0.13$ and $\Phi_{Cy3} = 0.12$ yielded orthogonal signals for the DHLA configurations. Minimal deviations from orthogonality were observed for variations in the quantum yields that were within ±0.02 of these values. The quantum yield values were also in good agreement with the average measured quantum yield for the QDs, $\langle\Phi_{QD}\rangle = 0.15 \pm 0.04$, as well as expectations for Cy3, which has reported quantum yields ranging from 0.04 to 0.39 for Cy3-labeled biomolecules,[57−60] albeit strongly dependent on local environment. In practice, QD and dye quantum yields can be directly measured or calibrated using suitable control samples (as we did here) to enable multiplexed sensing applications with combined CT-FRET. For empirical calibration, both sides of eq

DOI: 10.1021/jacs.6b11042
J. Am. Chem. Soc. 2017, 139, 363−372

5 can be multiplied by Φ_{QD} so that only the ratio Φ_{QD}/Φ_{dye} needs to be determined.

Other Potential Applications. The integration of CT and FRET with QDs may have value in many different (bio)-photonic applications. Given that concentric FRET configurations have relied on two distinct dye/QD PL ratios for their sensing capabilities,[16,23−25] it follows that the dye/QD PL ratio and $K(1 - \Phi_{CT})$ parameters could be used analogously in CT-FRET to enable multiplexed assays for the activity of proteases and other hydrolases, displacement assays for protein or DNA detection, and quantitative imaging methods. The use of a redox-active metal−ligand complex may also provide opportunities for chemical sensing that are not possible with concentric FRET systems, as well as opportunities for photoelectrochemical measurements. Alternatively, and drawing inspiration from what has been possible with time-gated lanthanide-to-QD-to-fluorescent dye FRET relays,[18,19] it may be possible to develop photonic logic probes using QDs with CT and FRET. Equally importantly, the fundamental understanding of combined CT and FRET developed in this study may have applicability beyond sensing. For example, nature has combined resonance energy transfer and charge transfer in photosynthetic systems,[61,62] such that CT-FRET with QDs may be a useful concept for artificial light harvesting and energy conversion. There are many interesting possibilities for configurations that can leverage the unique properties of a nanomaterial such as a QD with control over rates of CT and FRET.

CONCLUSIONS

We have shown that FRET and CT can concurrently and competitively quench QD PL. The competition between CT and FRET can be understood from a rate analysis, where the rates observed for configurations with only FRET and only CT are able to accurately predict quenching with the combination of CT and FRET, whether observed as the ensemble PL intensity or PL lifetime. Both ensemble and single particle PL measurements showed that the dye/QD PL was a function of FRET and approximately independent of CT, as predicted theoretically. The dye/QD PL ratio was combined with the quantum-yield-adjusted sum of the QD and dye PL intensities to potentiate orthogonal, multiplexed sensing through CT and FRET. This type of configuration is thus promising for applications in bioanalysis but may also be conceptually useful in other photonic applications.

METHODS

Materials. CdSe/ZnS QDs were synthesized[63,64] and coated with dihydrolipoic acid (DHLA) or poly(ethylene glycol)-appended dihydrolipoic acid (DHLA-PEG) ligands as described previously (see the Supporting Information for molecular structures of the ligands and TEM images of the QDs).[65,66] The concentration of the QDs was estimated by UV−visible spectrophotometry.[67,68] Alexa Fluor 555 C2 maleimide and Alexa Fluor 594 C5 maleimide were from ThermoFisher Scientific (Carlsbad, CA). Cyanine 3 maleimide was from GE Healthcare (Piscataway, NJ). Ruthenium(II) phenanthroline maleimide was synthesized as described previously.[69] Peptides were synthesized using standard *in situ* neutralization cycles with Boc-solid-phase peptide synthesis.[70,71] Peptides were labeled with maleimide derivatives of either ruthenium(II) phenanthroline or a fluorescent dye, and purified following previously published procedures.[71,72] Two peptide sequences were used: C*STRIDEANQRATKLP$_7$SH$_6$, which is abbreviated as Pep(*), where * represents a dye or ruthenium(II) phenanthroline label and the underlined residues are sites that can be hydrolyzed by trypsin, and C*-(Aib)$_6$G$_2$H$_6$, which is abbreviated by Lnk(*). QD-peptide conjugates were prepared by mixing 20 pmol of QDs with the desired number of equivalents of labeled peptide(s) dissolved in buffer to a final volume of 110 μL. No purification of the conjugates was needed because of the high efficiency of the binding of the polyhistidine (H_6) tag to the QDs.[50,51] Buffer solutions were phosphate buffer saline (PBS; 10 mM, 137 mM NaCl, 2.7 mM KCl) for DHLA-PEG-coated QDs and borate buffer (100 mM, pH 8.5) for DHLA-coated QDs.

Measurements. Absorbance and PL emission spectra were measured on an Infinite M1000 multifunction plate reader (Tecan Ltd., Morrisville, NC). The excitation wavelengths for measurement of PL emission spectra were 400 nm with A555 and Cy3 dyes and 450 nm with A594 dye. In the case of A555 and Cy3, direct excitation of dye fluorescence was negligible at the excitation wavelength. For A594, direct excitation was minimized but not negligible. Directly excited A594 fluorescence was subtracted from spectra using reference samples with only A594-labeled peptide. PL lifetime measurements were made using a 375 nm diode laser with 50 ps pulse widths operating at 20 MHz (Becker & Hickl GmbH, Berlin, Germany). PL emission was wavelength-selected using a SPEX 270 M spectrograph (Spex Industries, Edison, NJ), detected with a 8309U-50 MCP-PMT (Hamamatsu, Hamamatsu City, Japan), and processed with a time-correlated single-photon counting system (Becker & Hickl). PL decays were fit with biexponential functions using FluoFit software (PicoQuant, Berlin, Germany). Amplitude-weighted average lifetimes were calculated as described in the Supporting Information.

Single particle FRET measurements were done using an Axiovert inverted microscope (Zeiss, Peabody, MA).[73] Laser excitation (457 nm) was coupled into a single-mode optical fiber. The output from the fiber was tightly focused into the sample solution using a 100× neofluar objective lens (1.4 N.A., Zeiss). The fluorescence from the samples was focused onto a 75 μm pinhole to reject the out-of-focus emission. After the pinhole, QD and Cy3 PL were separated using a dichroic filter (FF552; Semrock, Rochester, NY) and detected using single-photon avalanche detectors (SPCM-ARQH-14, Excelitas, Waltham, MA). The fluorescence burst signals from each detector were collected using a counter/timer board (PCI-6602, National Instruments, Austin, TX). The laser power was adjusted to give a maximum burst level of ∼100 counts, which corresponded to an optical power <75 μW prior to the objective. The signals from each channel were corrected for crosstalk and processed into intensity ratio histograms using custom-designed software following a previously reported algorithm.[52] An event was counted when the sum of the burst signals from both channels exceeded a threshold of 30 counts.

ASSOCIATED CONTENT

Supporting Information

The Supporting Information is available free of charge on the ACS Publications website at DOI: 10.1021/jacs.6b11042.

Ligand structures, additional details on data analysis and calculations, spectral overlap integrals and calculation of Förster distances, TEM images of the QDs, PL intensity data for DHLA-PEG-coated QDs with Ru-phen/A555 and Ru-phen/A594 combinations, PL intensity and lifetime data for DHLA-coated QDs with Ru-phen/Cy3, Ru-phen/A555, and Ru-phen/A594 combinations, trypsin hydrolysis experiments with DHLA-coated QDs, single particle FRET data with DHLA-PEG coated QDs, investigation of quenching of dye PL, and orthogonal enzyme assays with DHLA-coated QDs (PDF)

AUTHOR INFORMATION

Corresponding Author

*algar@chem.ubc.ca

DOI: 10.1021/jacs.6b11042
J. Am. Chem. Soc. 2017, 139, 363−372

ORCID

W. Russ Algar: 0000-0003-3442-7072
Igor L. Medintz: 0000-0002-8902-4687

Notes

The authors declare no competing financial interest.

■ ACKNOWLEDGMENTS

W.R.A. thanks the Natural Sciences and Engineering Research Council of Canada (NSERC), the Canada Foundation for Innovation (CFI), and the University of British Columbia for support. W.R.A. is also grateful for a Canada Research Chair (Tier 2) and a Michael Smith Foundation for Health Research Scholar Award. I.L.M., J.S.M., and A.L.H. acknowledge NRL, the NRL Nanosciences Institute, the DoD Laboratory-University Collaboration Initiative, the Office of Naval Research, and the Defense Threat Reduction Agency for support. Amy M. Scott, at the University of Miami, is thanked for useful discussion.

■ REFERENCES

(1) Resch-Genger, U.; Grabolle, M.; Cavaliere-Jaricot, S.; Nitschke, R.; Nann, T. *Nat. Methods* **2008**, *5*, 763−775.
(2) Zrazhevskiy, P.; Seno, M.; Gao, X. H. *Chem. Soc. Rev.* **2010**, *39*, 4326−4354.
(3) Rosenthal, S. J.; Chang, J. C.; Kovtun, O.; McBride, J. R.; Tomlinson, I. D. *Chem. Biol.* **2011**, *18*, 10−24.
(4) Blanco-Canosa, J. B.; Wu, M.; Susumu, K.; Petryayeva, E.; Jennings, T. L.; Dawson, P. E.; Algar, W. R.; Medintz, I. L. *Coord. Chem. Rev.* **2014**, *263*−*264*, 101−137.
(5) Sperling, R. A.; Parak, W. J. *Philos. Trans. R. Soc., A* **2010**, *368*, 1333−1383.
(6) Mattoussi, H.; Palui, G.; Na, H. B. *Adv. Drug Delivery Rev.* **2012**, *64*, 138−166.
(7) Petryayeva, E.; Algar, W. R.; Medintz, I. L. *Appl. Spectrosc.* **2013**, *67*, 215−252.
(8) Wegner, K. D.; Hildebrandt, N. *Chem. Soc. Rev.* **2015**, *44*, 4792−4834.
(9) Das, A.; Snee, P. T. *ChemPhysChem* **2016**, *17*, 598−617.
(10) Tamang, S.; Lincheneau, C.; Hermans, Y.; Jeong, S.; Reiss, P. *Chem. Mater.* **2016**, *28*, 2491−2506.
(11) Dasog, M.; Kehrle, J.; Rieger, B.; Veinot, J. G. C. *Angew. Chem., Int. Ed.* **2016**, *55*, 2322−2339.
(12) Gonzalez, C. M.; Veinot, J. G. C. *J. Mater. Chem. C* **2016**, *4*, 4836−4846.
(13) Hildebrandt, N.; Spillman, C. M.; Algar, W. R.; Pons, T.; Stewart, M. H.; Oh, E.; Susumu, K.; Díaz, S. A.; Delehanty, J. B.; Medintz, I. L. *Chem. Rev.* **2016**, DOI: 10.1021/acs.chemrev.6b00030.
(14) Boeneman, K.; Prasuhn, D. E.; Blanco-Canosa, J. B.; Dawson, P. E.; Melinger, J. S.; Ancona, M.; Stewart, M. H.; Susumu, K.; Huston, A.; Medintz, I. L. *J. Am. Chem. Soc.* **2010**, *132*, 18177−18190.
(15) Spillmann, C. M.; Ancona, M. G.; Buckhout-White, S.; Algar, W. R.; Stewart, M. H.; Susumu, K.; Huston, A. L.; Goldman, E. R.; Medintz, I. L. *ACS Nano* **2013**, *7*, 7101−7118.
(16) Algar, W. R.; Malanoski, A. P.; Susumu, K.; Stewart, M. H.; Hildebrandt, N.; Medintz, I. L. *Anal. Chem.* **2012**, *84*, 10136−10146.
(17) Algar, W. R.; Wegner, D.; Huston, A. L.; Blanco-Canosa, J. B.; Stewart, M. H.; Armstrong, A.; Dawson, P. E.; Hildebrandt, N.; Medintz, I. L. *J. Am. Chem. Soc.* **2012**, *134*, 1876−1891.
(18) Claussen, J. C.; Algar, W. R.; Hildebrandt, N.; Susumu, K.; Ancona, M. G.; Medintz, I. L. *Nanoscale* **2013**, *5*, 12156−12170.
(19) Claussen, J. C.; Hildebrandt, N.; Susumu, K.; Ancona, M. G.; Medintz, I. L. *ACS Appl. Mater. Interfaces* **2014**, *6*, 3771−3778.
(20) Alam, R.; Zylstra, J.; Fontaine, D. M.; Branchini, B. R.; Maye, M. M. *Nanoscale* **2013**, *5*, 5303−5306.
(21) Dwyer, C. L.; Diaz, S. A.; Walper, S. A.; Samanta, A.; Susumu, K.; Oh, E.; Buckhout-White, S.; Medintz, I. L. *Chem. Mater.* **2015**, *27*, 6490−6494.
(22) Algar, W. R.; Ancona, M. G.; Malanoski, A. P.; Susumu, K.; Medintz, I. L. *ACS Nano* **2012**, *6*, 11044−11058.
(23) Wu, M.; Algar, W. R. *Anal. Chem.* **2015**, *87*, 8078−8083.
(24) Li, J. J.; Algar, W. R. *Analyst* **2016**, *141*, 3636−3647.
(25) Wu, M.; Petryayeva, E.; Algar, W. R. *Anal. Chem.* **2014**, *86*, 11181−11188.
(26) Diaz, S. A.; Giordano, L.; Azcarate, J. C.; Jovin, T. M.; Jares-Erijman, E. A. *J. Am. Chem. Soc.* **2013**, *135*, 3208−3217.
(27) Clapp, A. R.; Medintz, I. L.; Mauro, J. M.; Fisher, B. R.; Bawendi, M. G.; Mattoussi, H. *J. Am. Chem. Soc.* **2004**, *126*, 301−310.
(28) Medintz, I. L.; Clapp, A. R.; Mattoussi, H.; Goldman, E. R.; Fisher, B.; Mauro, J. M. *Nat. Mater.* **2003**, *2*, 630−638.
(29) Dennis, A. M.; Bao, G. *Nano Lett.* **2008**, *8*, 1439−1445.
(30) Lu, H.; Schops, O.; Woggon, U.; Niemeyer, C. M. *J. Am. Chem. Soc.* **2008**, *130*, 4815−4827.
(31) Suzuki, M.; Husimi, Y.; Komatsu, H.; Suzuki, K.; Douglas, K. T. *J. Am. Chem. Soc.* **2008**, *130*, 5720−5725.
(32) Charbonniere, L. J.; Hildebrandt, N.; Ziessel, R. F.; Loehmannsroeben, H. G. *J. Am. Chem. Soc.* **2006**, *128*, 12800−12809.
(33) Hildebrandt, N.; Charbonniere, L. J.; Beck, M.; Ziessel, R. F.; Lohmannsroben, H. G. *Angew. Chem., Int. Ed.* **2005**, *44*, 7612−7615.
(34) So, M. K.; Xu, C. J.; Loening, A. M.; Gambhir, S. S.; Rao, J. H. *Nat. Biotechnol.* **2006**, *24*, 339−343.
(35) Yao, H. Q.; Zhang, Y.; Xiao, F.; Xia, Z. Y.; Rao, J. H. *Angew. Chem., Int. Ed.* **2007**, *46*, 4346−4349.
(36) Algar, W. R.; Stewart, M. H.; Scott, A. M.; Moon, W. J.; Medintz, I. L. *J. Mater. Chem. B* **2014**, *2*, 7816−7827.
(37) Medintz, I. L.; Farrell, D.; Susumu, K.; Trammell, S. A.; Deschamps, J. R.; Brunel, F. M.; Dawson, P. E.; Mattoussi, H. *Anal. Chem.* **2009**, *81*, 4831−4839.
(38) Medintz, I. L.; Pons, T.; Trammell, S. A.; Grimes, A. F.; English, D. S.; Blanco-Canosa, J. B.; Dawson, P. E.; Mattoussi, H. *J. Am. Chem. Soc.* **2008**, *130*, 16745−16756.
(39) Scott, A. M.; Algar, W. R.; Stewart, M. H.; Trammell, S. A.; Blanco-Canosa, J. B.; Dawson, P. E.; Deschamps, J. R.; Goswami, R.; Oh, E.; Huston, A. L.; Medintz, I. L. *J. Phys. Chem. C* **2014**, *118*, 9239−9250.
(40) Sandros, M. G.; Shete, V.; Benson, D. E. *Analyst* **2006**, *131*, 229−235.
(41) Sandros, M. G.; Gao, D.; Benson, D. E. *J. Am. Chem. Soc.* **2005**, *127*, 12198−12199.
(42) Opperwall, S. R.; Divakaran, A.; Porter, E. G.; Christians, J. A.; DenHartigh, A. J.; Benson, D. E. *ACS Nano* **2012**, *6*, 8078−8086.
(43) Medintz, I. L.; Stewart, M. H.; Trammell, S. A.; Susumu, K.; Delehanty, J. B.; Mei, B. C.; Melinger, J. S.; Blanco-Canosa, J. B.; Dawson, P. E.; Mattoussi, H. *Nat. Mater.* **2010**, *9*, 676−684.
(44) Freeman, R.; Finder, T.; Gill, R.; Willner, I. *Nano Lett.* **2010**, *10*, 2192−2196.
(45) Ruedas-Rama, M. J.; Hall, E. A. H. *Nanotechnology* **2014**, *25*, 195501.
(46) Ruedas-Rama, M. J.; Hall, E. A. H. *Anal. Chem.* **2008**, *80*, 8260−8268.
(47) Harris, R. D.; Homan, S. B.; Kodaimati, M.; He, C.; Nepomnyashchii, A. B.; Swenson, N. K.; Lian, S.; Calzada, R.; Weiss, E. A. *Chem. Rev.* **2016**, *116*, 12865−12919.
(48) Algar, W. R.; Tavares, A. J.; Krull, U. J. *Anal. Chim. Acta* **2010**, *673*, 1−25.
(49) Algar, W. R.; Malanoski, A.; Deschamps, J. R.; Blanco-Canosa, J. B.; Susumu, K.; Stewart, M. H.; Johnson, B. J.; Dawson, P. E.; Medintz, I. L. *Nano Lett.* **2012**, *12*, 3793−3802.
(50) Sapsford, K. E.; Pons, T.; Medintz, I. L.; Higashiya, S.; Brunel, F. M.; Dawson, P. E.; Mattoussi, H. *J. Phys. Chem. C* **2007**, *111*, 11528−11538.
(51) Aldeek, F.; Safi, M.; Zhan, N. Q.; Palui, G.; Mattoussi, H. *ACS Nano* **2013**, *7*, 10197−10210.

DOI: 10.1021/jacs.6b11042
J. Am. Chem. Soc. 2017, 139, 363−372

(52) Pons, T.; Medintz, I. L.; Wang, X.; English, D. S.; Mattoussi, H. *J. Am. Chem. Soc.* **2006**, *128*, 15324−15331.
(53) Prasuhn, D. E.; Deschamps, J. R.; Susumu, K.; Stewart, M. H.; Boeneman, K.; Blanco-Canosa, J. B.; Dawson, P. E.; Medintz, I. L. *Small* **2010**, *6*, 555−564.
(54) Wu, M.; Massey, M.; Petryayeva, E.; Algar, W. R. *J. Phys. Chem. C* **2015**, *119*, 26183−26195.
(55) Braslavsky, S. E. *Pure Appl. Chem.* **2007**, *79*, 293−465.
(56) Boulesbaa, A.; Huang, Z. Q.; Wu, D.; Lian, T. Q. *J. Phys. Chem. C* **2010**, *114*, 962−969.
(57) Harvey, B. J.; Perez, C.; Levitus, M. *Photochem. Photobiol. Sci.* **2009**, *8*, 1105−1110.
(58) Massey, M.; Algar, W. R.; Krull, U. J. *Anal. Chim. Acta* **2006**, *568*, 181−189.
(59) Mujumdar, R. B.; Ernst, L. A.; Mujumdar, S. R.; Lewis, C. J.; Waggoner, A. S. *Bioconjugate Chem.* **1993**, *4*, 105−111.
(60) Randolph, J. B.; Waggoner, A. S. *Nucleic Acids Res.* **1997**, *25*, 2923−2929.
(61) Andrews, D. L.; Curutchet, C.; Scholes, G. D. *Laser Photon. Rev.* **2011**, *5*, 114−123.
(62) Vangrondelle, R.; Dekker, J. P.; Gillbro, T.; Sundstrom, V. *Biochim. Biophys. Acta, Bioenerg.* **1994**, *1187*, 1−65.
(63) Clapp, A. R.; Goldman, E. R.; Mattoussi, H. *Nat. Protoc.* **2006**, *1*, 1258−1266.
(64) Snee, P. T.; Chan, Y. H.; Nocera, D. G.; Bawendi, M. G. *Adv. Mater.* **2005**, *17*, 1131−1136.
(65) Mei, B. C.; Susumu, K.; Medintz, I. L.; Delehanty, J. B.; Mountziaris, T. J.; Mattoussi, H. *J. Mater. Chem.* **2008**, *18*, 4949−4958.
(66) Mei, B. C.; Susumu, K.; Medintz, I. L.; Mattoussi, H. *Nat. Protoc.* **2009**, *4*, 412−423.
(67) Yu, W. W.; Qu, L. H.; Guo, W. Z.; Peng, X. G. *Chem. Mater.* **2003**, *15*, 2854−2860.
(68) Jasieniak, J.; Smith, L.; van Embden, J.; Mulvaney, P.; Califano, M. *J. Phys. Chem. C* **2009**, *113*, 19468−19474.
(69) Trammell, S. A.; Goldston, H. M.; Tran, P. T.; Tender, L. M.; Conrad, D. W.; Benson, D. E.; Hellinga, H. W. *Bioconjugate Chem.* **2001**, *12*, 643−647.
(70) Schnolzer, M.; Alewood, P.; Jones, A.; Alewood, D.; Kent, S. B. H. *Int. J. Pept. Protein Res.* **1992**, *40*, 180−193.
(71) Algar, W. R.; Blanco-Canosa, J. B.; Manthe, R. L.; Susumu, K.; Stewart, M. H.; Dawson, P. E.; Medintz, I. L. *Methods Mol. Biol.* **2013**, *1025*, 47−73.
(72) Sapsford, K. E.; Farrell, D.; Sun, S.; Rasooly, A.; Mattoussi, H.; Medintz, I. L. *Sens. Actuators, B* **2009**, *139*, 13−21.
(73) Buckhout-White, S.; Spillmann, C. M.; Algar, W. R.; Khachatrian, A.; Melinger, J. S.; Goldman, E. R.; Ancona, M. G.; Medintz, I. L. *Nat. Commun.* **2014**, *5*, 5615.

DOI: 10.1021/jacs.6b11042
J. Am. Chem. Soc. 2017, 139, 363−372